

Modeling Cosmogenic ^{10}Be During the Heliosphere's Encounter with an Interstellar Cold Cloud

Anna Nica¹, Merav Opher¹, Jesse Miller¹, Jennifer L. Middleton²

¹Boston University Department of Astronomy, Boston University, Boston, MA, USA

²Lamont-Doherty Earth Observatory, Columbia University, Palisades, NY, USA

Key Points:

- Crossing massive interstellar cold clouds exposes Earth to a higher energetic particle flux that increases atmospheric production of ^{10}Be
- An AU-scale cold cloud can be detected in ocean sediments if Earth receives energetic particles from crossing the compressed heliosphere
- A sub-pc-scale cold cloud cannot be detected in Fe-Mn crusts if Earth is only exposed to interstellar fluxes of galactic cosmic rays

Abstract

Geologic records of cosmogenic ^{10}Be are sensitive to changes in the radiation environment with time. Recent works suggest there are periods when the Sun encountered massive cold clouds which compressed the heliosphere to within Earth's orbit. This would expose Earth to increased galactic cosmic rays and MeV-energy particles of heliospheric origin. We model ^{10}Be production in Earth's atmosphere during possible cold cloud encounters, and estimate their detectability in marine records of variable temporal resolution. We find that an AU-scale cold cloud encounter can be detected using ocean sediment measurements of ^{10}Be if Earth spends time inside the compressed heliosphere. For typical relative speeds between the Sun and local interstellar clouds, this translates to a crossing time of ~ 100 years. A cloud must have an extension on the scale of parsecs to tens-of-parsecs (crossing time 0.1-1 Myr) to be detectable through ^{10}Be measurements in iron-manganese crusts.

Plain Language Summary

The solar wind forms the heliosphere as the Sun moves through the interstellar medium and surrounds the Solar System. As the Sun moves through the galaxy, it can encounter dense, cold interstellar clouds that compress the heliosphere. This exposes Earth to more galactic cosmic rays from the galaxy, and energetic particles accelerated in the compressed heliosphere. This produces more of the radioisotope ^{10}Be in Earth's atmosphere, which is deposited in deep-sea sediments and mineral crusts growing on the seafloor. Marine geologic archives of ^{10}Be can record when exposures to high radiation occurred millions of years ago. We calculate the rate of ^{10}Be production that would occur on Earth during the heliosphere's encounter with a dense interstellar cold cloud. We find that crossing through an AU-size cloud can be detected by ^{10}Be measurements in ocean sediments only if Earth is exposed to energetic particles as it orbits in and out of the compressed heliosphere. For typical relative speeds between the Sun and interstellar clouds, this corresponds to a crossing time of ~ 100 years. Cold cloud encounters can be detected by measuring ^{10}Be in deep-ocean crusts and sediments if the cloud size is on the parsec scale (crossing time 100,000-1 million years). We find that such an encounter can be detected in marine records if the cloud has an extension of ~ 2 pc, and Earth spends time inside the compressed heliosphere. If the cloud has an extension of ~ 0.2 pc, cloud crossings cannot be distinguished from typical variability.

1 Introduction

The Sun moves with a speed of 19 km/s relative to nearby stars, carrying the Solar System through diverse regions of the interstellar medium (ISM) with different densities, temperatures, and compositions. As the Sun travels, the solar wind engulfs the Solar System in a protective bubble known as the heliosphere. The heliosphere shields Earth from interstellar galactic cosmic rays (GCRs) that are accelerated by high-energy events occurring elsewhere in the galaxy. Voyager spacecraft observations have shown that the heliosphere deflects 80% of GCRs with energies 70 MeV - 5 GeV (Cummings et al., 2016; Stone et al., 2019) at its outer boundary.

The shape and size of the heliosphere depends on the pressure balance between the outflowing solar wind and the surrounding ISM. Today, the heliopause extends to ~ 120 AU in the Sun's direction of motion when the neutral H density of the ISM is ~ 0.1 - 0.2 cm^{-3} (Stone et al., 2013, 2019). However, this size could have changed dramatically if the Solar System passed through dense, cold interstellar clouds with densities $\geq 900 \text{ cm}^{-3}$. After tracing the trajectory of the Solar System back several million years, Opher, Loeb, Zucker, et al. (2024) and Opher, Loeb, & Peek (2024) predict that the Solar System may have traversed dense interstellar cold clouds or regions 2-3 Mya and 6-7 Mya, respectively. These works have shown that, in the event of such crossings, these high densities can col-

lapse the heliosphere to < 1 AU in the nose direction. This would expose Earth to high fluxes of varied radiation in the form of GCRs and solar energetic particles for the duration of the cloud crossing (Opher, Giacalone, et al., 2025, in review). Earth's dipole magnetic field can deflect particles with energies up to 15 GeV near the geomagnetic equator, however high fluxes of these MeV-range GCRs and solar energetic particles can still enter Earth's atmosphere near the poles (Comedi et al., 2020).

Cosmogenic isotopes, such as ^{10}Be , are produced when cosmic rays and energetic particles collide with molecules in Earth's atmosphere and induce nucleonic-muon-electromagnetic cascades (Poluianov et al., 2016; Miyake et al., 2012; Lal & Peters, 1967). ^{10}Be has a half-life of 1.4 million years (Myr), which is long enough to detect radiation changes within the past 12 Myr (Willenbring & von Blanckenburg, 2010). ^{10}Be produced in Earth's atmosphere is deposited on the ocean floor, and remains detectable thousands-to-millions of years later through sampling of marine sediments and deep-ocean iron-manganese crusts (Willenbring & von Blanckenburg, 2010; Simon et al., 2018). Prolonged exposure to increased radiation should increase cosmogenic radionuclide production in Earth's atmosphere, and thus may be recorded in geologic archives of these isotopes, with the duration depending on the size of the interstellar cold cloud.

The detectability of a cold cloud encounter using cosmogenic isotopes has been explored within lunar soil samples and terrestrial iron-manganese crusts recovered from the seafloor, though these methods are limited by the timing and duration of the crossing. Poluianov & Engelbrecht (2025) model the ^{26}Al signal produced by an interstellar cloud encounter that would be detectable in lunar soil samples. ^{26}Al has a half-life of ~ 0.7 Myr (Poluianov et al., 2018), making it another cosmogenic isotope ideal for observing cold cloud crossings several million years ago. Poluianov & Engelbrecht (2025) find no evidence that the heliosphere crossed through an interstellar cold cloud 2-4 Mya, but the authors suggest that cloud crossings shorter than a few tens of thousands of years would be undetectable with this approach. A cloud crossing event would need to last ~ 100 kyrs to be detectable in existing lunar soil data, but shorter crossings could be detected using modern, higher-precision sampling techniques. It is not clear if the signal of the proposed cold cloud crossing between 2-3 Mya can be detected in records of ^{10}Be , as the cloud size is currently unknown (Opher, Loeb, et al., 2025, in review). Cold clouds in our interstellar neighborhood, such as the Local Leo Cold Cloud, could be thin sheets that are only 200 AU ($\sim 10^{-3}$ pc) across (Meyer et al., 2012). Vannier et al. (2025) argue based on UV observations that cold clouds within the Local Ribbon might be very small, and Peek et al. (2025) argue that the clouds may be filamentary. This could result in a crossing time that is less than 100 years, or periodic compressions of the heliosphere that yield short-lived increases in ^{10}Be production. On the other hand, Koll et al. (2025) detect a prolonged increase in ^{10}Be production 10 Mya lasting 1-2 Myrs and suggest an interstellar cold cloud crossing as a possible explanation. A 1-2 Myr crossing event could correspond to a cloud that is tens of parsecs across.

In this work, we use the Cosmic Ray Atmospheric Cascade model for atmospheric production of cosmogenic isotopes (Poluianov et al., 2016) to predict the production rates of ^{10}Be on Earth during possible encounters with interstellar cold clouds. The detectability of a cloud crossing—and subsequent heliospheric compression—in the geologic record depends on the size, temperature, density, and relative velocity of the cloud. This work determines how increased radiation induced by an interstellar cold cloud could affect ^{10}Be production on Earth. We explore several potential crossing times and evaluate whether such an event can be detected in terrestrial archives.

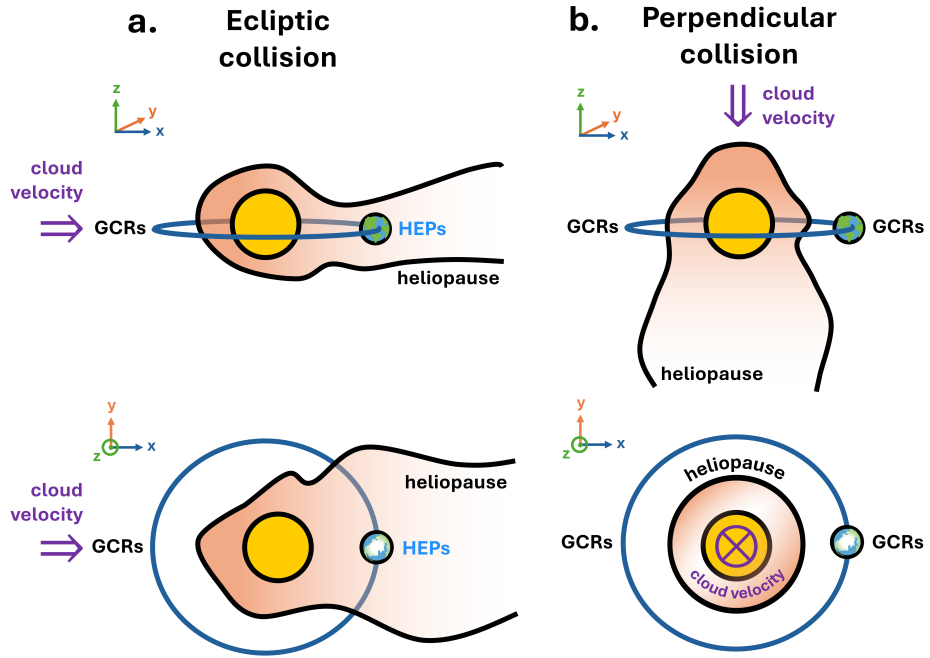


Figure 1. Cartoon diagram showing compression of the heliosphere and Earth's exposure to energetic particles as the Solar System intersects an interstellar cold cloud. Panel a shows heliospheric compression following a collision with a cold cloud in the ecliptic plane, from an edge-on and top-down view. Earth's orbit dips in and out of the heliosphere, exposing Earth to interstellar GCRs while it is outside the heliosphere and to HEPs inside the heliosphere. Panel b shows heliospheric compression if the cloud's relative velocity is perpendicular to the ecliptic plane. In this case, the heliosphere may be compressed within Earth's orbit, and Earth would only be exposed to interstellar GCRs.

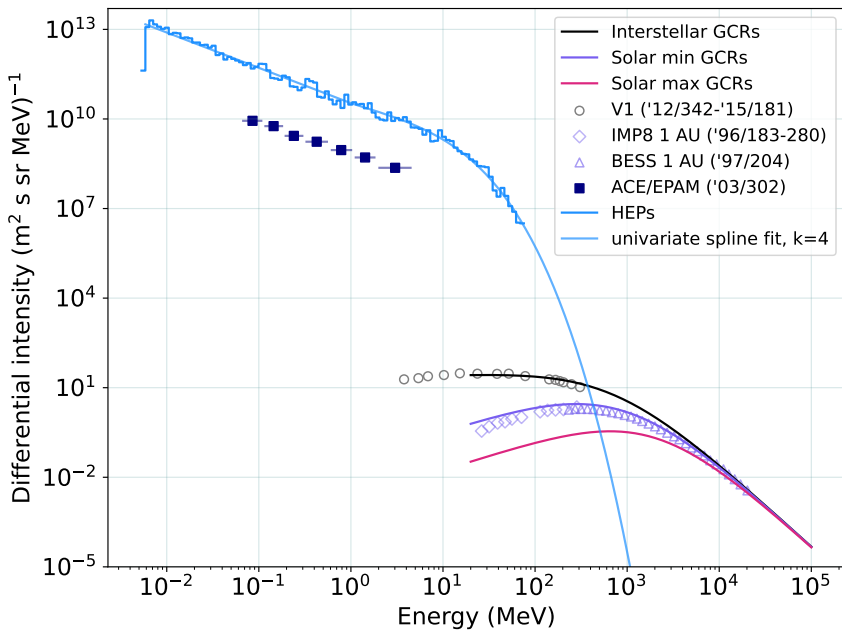


Figure 2. Proton differential energy spectra of the heliospheric energetic particle (HEP) flux as shown by Opher, Giacalone, et al. (2025, in review) and applied fit function (blue line), interstellar flux of GCRs (black line), GCRs modulated for typical solar minimum conditions (purple line), and typical solar maximum conditions (pink line). Black circles represent cosmic ray detections from Voyager 1 after exiting the heliosphere, from DOY 342 of 2012 to DOY 181 of 2015. Purple points represent data from a BESS balloon flight in 1997 and from IMP8 in 1996. These data are shown as in Cummings et al. (2016). Navy squares show SEP fluxes during the Halloween Storm of 2003, one of the largest recorded solar storms (Mewaldt et al., 2005).

2 Model Description

2.1 Heliosphere and Radiation Model

Compression of the heliosphere during a cold cloud crossing would depend on the velocity of the cloud relative to the Sun. We consider two possibilities: a collision with a cold cloud in the ecliptic plane and a collision perpendicular to the ecliptic plane (Figure 1). An ecliptic collision is an example of an event where Earth would spend a portion of its orbit inside the heliosphere and a portion outside the heliosphere (Figure 1a). In a perpendicular collision (Figure 1b), if the heliosphere is sufficiently compressed to within Earth's orbit, Earth would be continuously exposed to interstellar space. Because the dimensions of the cold clouds are not known, we consider cloud crossing times between 100 years and 1 Myr. This can correspond to clouds on hundreds-of-AU scales to tens-of-parsecs scales. Cloud sizes are based on a nominal speed between the cloud and the Sun of 20 km/s (Opher, Loeb, & Peek, 2024; Opher, Loeb, Zucker, et al., 2024).

In both cases, Earth would spend time outside the heliosphere, experiencing interstellar fluxes of GCRs. We assume minimal attenuation of GCRs by the cold cloud: a 1 GeV proton has a mean free path of 2700 pc, making collisions with hydrogen atoms within even a 20-pc cloud unlikely. Morlino & Gabici (2015) find a \sim 10% reduction in flux for GCRs with energies 100 MeV within a cloud with a column density similar to the estimated size of the Local Leo Cold Cloud (Meyer et al., 2012). Our resulting ^{10}Be production rates may differ by \sim 10% in the upper atmosphere, depending on the extent of the cloud.

In the case of an ecliptic collision, Earth would re-enter the heliosphere for part of its orbit and be exposed to heliospheric energetic particles (HEPs) during this time (Opher, Giacalone, et al., 2025, in review). HEPs are produced when energetic particles in the solar wind are accelerated at the termination shock of the compressed heliosphere. In a compressed heliosphere, the termination shock becomes a parallel shock. The termination shock is also much stronger (shock compression of 4) and accelerates high fluxes of energetic particles from keV to MeV energies (Opher, Giacalone, et al., 2025, in review). As shown in Figure 2, the flux of HEPs at MeV energies is at least \sim 6 orders of magnitude greater than the flux of interstellar GCRs. The HEP flux is 1-2 orders of magnitude greater than the energetic particle flux of the largest recorded solar storm: the Halloween Storm of 2003 (Mewaldt et al., 2005). While effects from solar storms can last days to weeks, Earth's exposure to HEPs would occur for several months each year while the heliosphere crosses through the cold cloud.

2.2 ^{10}Be Production Model

We compute the production of ^{10}Be using the CRAC (Cosmic Ray Atmospheric Cascade) model developed by Poluijanov et al. (2016) and validated by Golubenko et al. (2021). This model numerically calculates yield functions of ^{10}Be using the GEANT4 simulation (Allison et al., 2006; Agostinelli et al., 2003) for primary protons and α -particles with energies 20 MeV-100 GeV. The model has an altitude range from 0-35 km, with an integrated bin for the upper atmosphere set at 100 km. The production rate Q is defined as

$$Q(t, h, R_c) = \sum_i \int_{E_{c,i}}^{\infty} Y_i(E, h) \cdot J_i(E, t) \cdot dE, \quad (1)$$

where the yield function $Y_i(E, h)$ for each species i depends on energy E and atmospheric depth h , and the energy spectrum $J_i(E, t)$ depends on particle energy and time. Integration over energy begins above the energy cutoff $E_{c,i}$ for each species, which depends on geomagnetic field parameters.

We apply a geomagnetic dipole moment $M = 7.8 \cdot 10^{22}$ Am², which is consistent with paleointensity data from the present day, to the Plio-Pleistocene era (Asefaw et al., 2021; Biggin et al., 2010).

For the spectrum of interstellar GCRs, we use the parametrization by Vos & Potgieter (2015) fit to Voyager 1 measurements (Stone et al., 2013). Modulation of GCR fluxes as the heliosphere changes throughout the solar cycle is parameterized using the modulation potential $\phi(t)$ (Caballero-Lopez & Moraal, 2004).

The HEP spectrum is based on a model that solves the Parker transport equation at the termination shock of a compressed heliosphere (Opher, Giacalone, et al., 2025, in review). We estimate a univariate spline fit of degree 4 to extrapolate fluxes at higher energies (Figure 2).

2.3 Experiment Setup

We determine cosmogenic ¹⁰Be production for five cases: solar maximum (solar modulation potential $\phi = 1100$ MV), solar minimum ($\phi = 325$ MV), average solar modulation across a typical solar cycle ($\phi = 500$ MV), exposure to interstellar GCRs while Earth is outside the compressed heliosphere ($\phi = 0$ MV), and exposure to HEPs while Earth re-enters the compressed heliosphere. We hold the geomagnetic field strength constant at present-day values. We consider cloud crossing periods lasting 100 years (~ 400 AU-wide cloud), 0.1 Myr (2 pc cloud), and 1 Myr (20 pc cloud). We determine ¹⁰Be production during an event where Earth enters and exits the heliosphere, estimating that Earth is exposed to interstellar GCRs for 80% of its orbit and to HEPs for 20% of its orbit (Opher, Giacalone, et al., 2025, in review). These proportions match the heliospheric model presented by Opher, Loeb, & Peek (2024), though exposure to HEPs and GCRs can change depending on the direction the Sun encounters a cold cloud and the shape of the heliosphere's tail. We repeat this process for a perpendicular collision, where Earth is exposed only to interstellar GCRs for its entire orbit. We do not account for atmospheric mixing (Heikkilä et al., 2009; Zheng et al., 2024).

3 Results

Particle Type	Global ¹⁰ Be prod. rate [atoms cm ⁻² s ⁻¹]	Polar ¹⁰ Be prod. rate [atoms cm ⁻² s ⁻¹]
Solar max GCRs	2.31×10^{-2}	4.84×10^{-2}
Avg solar cycle GCRs	3.39×10^{-2}	8.51×10^{-2}
Solar min GCRs	3.91×10^{-2}	1.06×10^{-1}
Interstellar GCRs	5.52×10^{-2}	1.78×10^{-1}
HEPs	9.15×10^0	1.23×10^2

Table 1. Polar (90°) and globally-averaged ¹⁰Be production rates for GCRs at three stages of the solar cycle under modern-day heliospheric conditions, GCRs in the interstellar medium, and heliospheric energetic particles (HEPs).

We calculate columnar and global production rates as in Poluianov et al. (2016). In Table 1, we determine the globally-averaged ¹⁰Be deposition rates and deposition at latitude 90°. Throughout the solar cycle, the polar production rate fluctuates between 0.05-0.1 atoms cm⁻² s⁻¹ ($2-3 \times 10^9$ atoms cm⁻² kyr⁻¹). The average present-day production rate is within the range of previous ¹⁰Be production rate estimates of Masarik

& Beer (2009). The polar production rate from GCRs outside the heliosphere increases by a factor of 1.63 from the average point of the solar cycle. To validate our implementation of the model, we compare our results for GCR-induced ^{10}Be production at each point in the solar cycle and in the interstellar GCRs case. Our results for globally-averaged GCR-induced ^{10}Be production throughout the solar cycle and outside the heliosphere are within 6% of the global production determined by Poluianov et al. (2016) and Pavlov et al. (2017) using similar models.

The presence of HEPs dramatically increases ^{10}Be production rates. HEP-induced polar ^{10}Be production increases by a factor of 1450 compared to the average point of the solar cycle. The HEP-induced globally-averaged ^{10}Be production increases by a factor of 270 from the average point of a modern-day solar cycle. Because we do not include atmospheric mixing, these production values over-predict the polar HEP-induced ^{10}Be deposition. Atmospheric models suggest that 50-80% of ^{10}Be produced at latitudes 60-90°N is deposited at latitudes lower than 60°N; conversely, ^{10}Be produced at lower latitudes can be deposited near the poles (Heikkilä et al., 2009; Zheng et al., 2024). Since HEPs are confined to MeV energies and lower, they do not penetrate geomagnetic shielding at equatorial latitudes, so HEP-induced ^{10}Be production occurs only near the poles. Measurements taken at ice core sites in Greenland or Antarctica may therefore see HEP-induced ^{10}Be deposition rates that are 20-50% lower than the polar production rates we compute.

While a cold cloud encounter could increase ^{10}Be production in Earth's atmosphere, its detectability in deep-ocean sediments and iron-manganese crusts depends on the duration of the event, terrestrial variability in ^{10}Be production and deposition, and exposure to HEPs and GCRs. In Figure 3, we show a time series of the ^{10}Be production rate while Earth was exposed to HEPs and GCRs (similar to the ecliptic collision in Figure 1a). We model a cloud crossing that may have occurred 2-3 Mya, such as the crossing of the Local Lynx of Cold Clouds suggested by Opher, Loeb, & Peek (2024), though our results can be generalized to other cloud crossing events. Outside the cloud, we calculate ^{10}Be production induced by GCRs at the average modulation of the solar cycle, assuming the heliosphere and ISM had similar size and density to today. During the cloud crossing, we assume a ratio of 80% interstellar GCR exposure to 20% HEP exposure per year on Earth, based on heliosphere simulations by Opher, Loeb, & Peek (2024) and Opher, Giacalone, et al. (2025, in review). This corresponds to HEP exposure for over 2 months each year. We then calculate the time-integrated ^{10}Be signal that would be recorded in marine archives using typical time resolutions for ocean sediments and iron-manganese crusts. Seafloor deposits of ^{10}Be can be measured as ^{10}Be flux or as $^{10}\text{Be}/^{9}\text{Be}$ ratios, from which changes to the ^{10}Be production rate can be inferred.

Ocean sediments accumulate at a rate scale of 1-10 cm/kyr. Each ^{10}Be measurement typically integrates 1 cm of material, yielding a time integration of ~ 1 kyr or shorter per sample. Changes in ^{10}Be production are driven by varying geomagnetic field intensity, and changes in ^{10}Be deposition are driven by climatic and environmental parameters occurring on thousand to hundred-thousand year timescales. Therefore, changes in ^{10}Be production and deposition induce a 2-4 \times typical variability in the ^{10}Be signal recorded by marine sediments (Frank et al., 1997; Simon et al., 2018; Middleton et al., 2025, in review). Iron-manganese crusts accumulate much more slowly at a rate scale of 1-5 mm/Myr, with each ^{10}Be measurement typically integrating 1 mm of material. This yields a ~ 200 -1000 kyr (0.2-1 Myr) time integration per sample. Integrating over these longer timescales, ^{10}Be data from iron-manganese crusts typically exhibit terrestrial variability on the order of 1-2 \times (Willenbring & von Blanckenburg, 2010).

We find that ^{10}Be can increase by a factor of 70 during a cold cloud crossing in which Earth is exposed to interstellar GCRs, with a ~ 2 -month exposure to HEPs. Detectability of this crossing depends on its duration. A short crossing on the order of 100 years (~ 400 AU cloud extension at a 20 pc/Myr relative velocity) may be detectable beyond

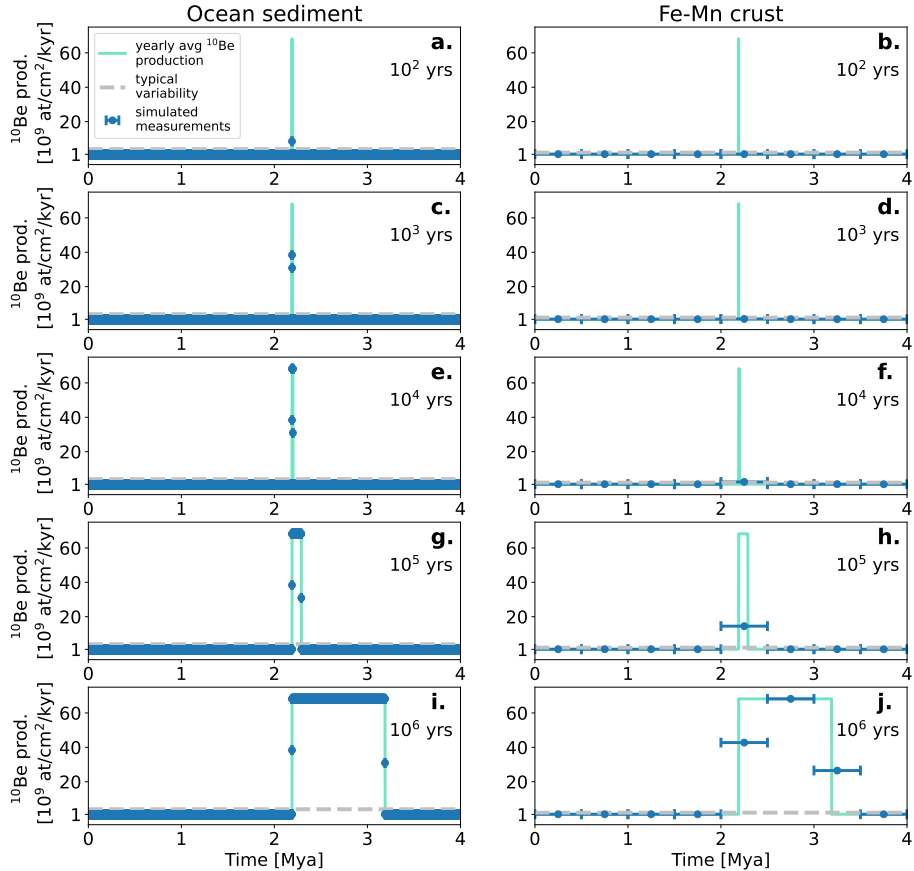


Figure 3. Simulated ^{10}Be signal during an ecliptic collision with a cold cloud (Figure 1a). We consider cloud crossing times between 10^2 years and 10^6 years. Turquoise lines show the modeled ^{10}Be production rate over time from 80% GCRs and 20% HEPs, and blue points show simulated measurements in ocean sediments (left, time resolution=1 kyr) and iron-manganese crusts (right, time resolution=0.5 Myr) based on the modeled production rates. Dashed gray lines show the upper range of typical variability in ^{10}Be recorded in marine archives due to dynamic terrestrial processes (Willenbring & von Blanckenburg, 2010; Simon et al., 2018; Middleton et al., 2025, in review).

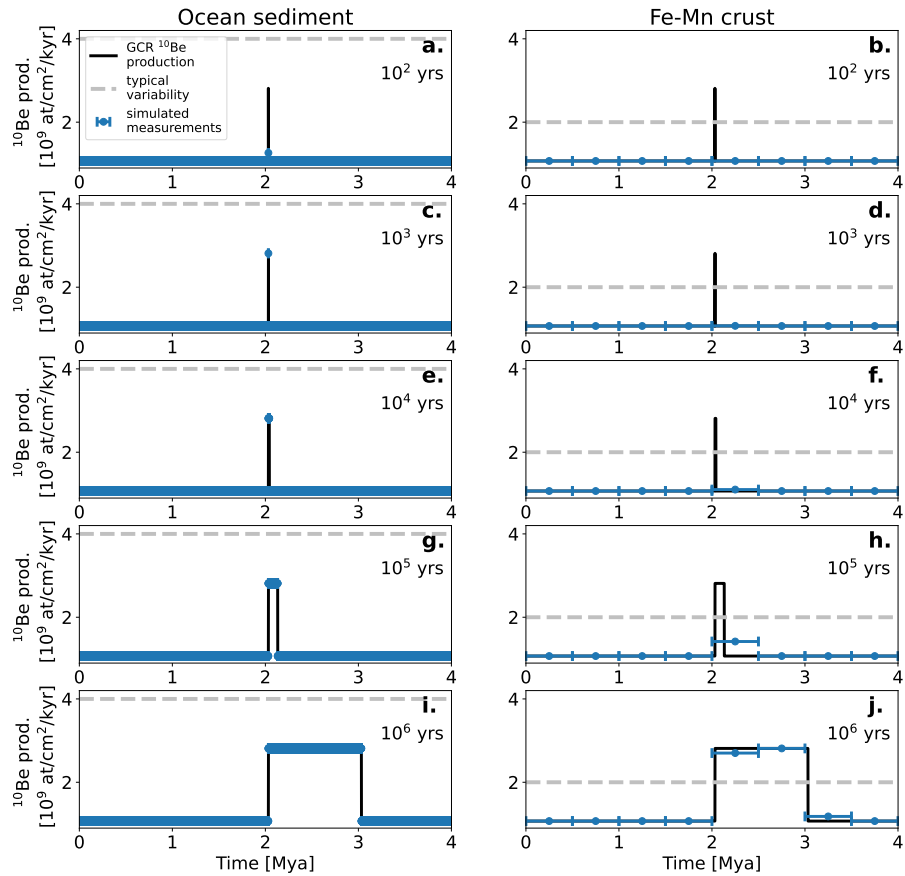


Figure 4. Similar to Figure 3, but for a perpendicular collision with a cold cloud (Figure 1b). Before the cold cloud crossing, the ^{10}Be production rate is set to the average modulation of GCRs throughout the solar cycle. During the crossing, the ^{10}Be production rate is induced by the interstellar flux of GCRs.

typical variability in ocean sediments, but is not detectable in iron-manganese crusts (Figures 3a, 3b). If the crossing lasts on the order of 100 kyr (0.1 Myr, ~ 2 pc cloud extension), it would produce an elevated ^{10}Be production signal spanning ~ 1 m of sediment (or 100 samples at a 1 cm sampling resolution). A high density of measurements across a peak can allow for more detailed characterization of the nature of the crossing and the cold cloud's structure. In comparison, this scenario would produce an elevated ^{10}Be production signal in only a few mm of iron-manganese crust (or 1-2 samples at a 1 mm sampling resolution), which limits any detailed characterization. A crossing lasting on the order of 1 Myr (~ 20 pc cloud extension) should enable multiple detections from both types of archives, at typical sampling resolution, if the HEP-induced signal is as high as $70\times$.

In Figure 4, we show the ^{10}Be production rate over time for a perpendicular collision where the heliosphere is compressed completely within Earth's orbit, and Earth is exposed only to interstellar GCRs (as in Figure 1b). In this case, the ^{10}Be production increases by less than a factor of 3 during the cloud crossing. This is completely within the scope of typical terrestrial variability for ocean sediments, making such a crossing signal harder to identify. Our model finds that a cloud crossing cannot be detectable in iron-manganese crusts if the event lasts 0.1 Myr because the ^{10}Be signal would be smoothed out within the 0.5 Myr integration time of a single iron-manganese 1mm sample. A cloud crossing where Earth is only exposed to interstellar GCRs could be detectable if the event lasts close to 1 Myr. However, this signal may be more difficult to distinguish from terrestrial causes that could also produce a long, low peak.

4 Discussion

Comparing the marine sample predictions in Figures 3 and 4, it is evident that prolonged and periodic exposure to HEPs is necessary for cold cloud encounters lasting less than ~ 1 Myrs to be detectable in ocean sediments and in iron-manganese crusts. An event lasting as short as 5-10 kyr could be resolved using ocean sediment records, if the timing of the event can be constrained to narrow the sampling period. A 10 kyr 20% HEP/80% GCR signal cannot be detected in iron-manganese crust records due to the signal's short duration relative to the samples' 500-kyr time integrations.

Detectability of a cold cloud encounter also depends on the density and extension of the cloud. If the heliosphere crossed through a very thin or filamentary cloud, a crossing event may have occurred on a timescale of ~ 100 years and would not be detectable in iron-manganese crust records. We find that high-resolution archives, such as those available in ocean sediment cores, are necessary to detect such a short-lived encounter. Long-lived encounters, on the other hand, may have their detectability compromised if the cold cloud has a high enough density to attenuate GCRs to within typical variability.

As discussed in Section 1, Poluianov & Engelbrecht (2025) find that lunar samples of ^{26}Al can only detect crossing events lasting ~ 100 kyr. At a relative velocity of 20 pc/Myr, this would require a crossing through a ~ 2 pc cold cloud. Similarly, we find that a crossing must last on the order of 100 kyr-1 Myr to be detected using iron-manganese crust samples of ^{10}Be . Koll et al. (2025) also do not see anomalous increases of ^{10}Be in iron-manganese crusts 2-3 Mya or 6-7 Mya, as proposed by Opher, Loeb, & Peek (2024) and Opher, Loeb, Zucker, et al. (2024). Our results suggest that, if cloud crossings occurred 2-3 or 6-7 Mya, they would need to have lasted on the order of 10^4 years or shorter as to not be detected using these archives. However, events lasting as short as 100-1000 years (corresponding to cloud extensions between hundreds to thousands of AU) could be detected using ocean sediment measurements if Earth is exposed to HEPs.

Koll et al. (2025) do report a prolonged increase in ^{10}Be concentrations in iron-manganese crusts around 9-11 Mya that could be attributed to an interstellar cold cloud crossing.

These measurements are elevated beyond typical variability for \sim 1-2 Myr, and the peak detection is a factor of 1.7 greater than background measurements. If this increase in concentration can be attributed to an increase in flux during a cold cloud crossing, this data would be consistent with our interstellar GCRs case (Figure 4f). If a cloud crossing occurred during this time, it may have compressed the heliosphere such that Earth was exposed mostly to interstellar GCRs and minimally to HEPs.

5 Summary

We model the production of cosmogenic radioisotope ^{10}Be in Earth's atmosphere when the heliosphere crosses through an interstellar cold cloud. A cold cloud encounter compresses the heliosphere and exposes Earth to increased radiation. We consider a case where the heliosphere is compressed such that Earth is exposed to pristine interstellar GCRs and HEPs, and a case where Earth is exposed only to interstellar GCRs. Interstellar GCRs increase the ^{10}Be production rate by less than a factor of 2 compared to typical solar cycle variation. HEPs increase the global production rate by a factor of 270, almost exclusively at polar latitudes. This results in a globally-averaged ^{10}Be production rate that increases by almost a factor of 70 from typical, non-compressed heliosphere conditions if Earth is exposed to HEPs for 20% of its annual orbit. The ratio of HEP to GCR exposure can vary depending on the shape of the heliosphere and the relative direction between the Sun and the cloud, though exposure to HEPs for a minority of Earth's orbit can still substantially increase ^{10}Be production.

Despite these increases in ^{10}Be production, detectability of a cold cloud crossing is not guaranteed. Detectability in marine records depends on the duration of the crossing, radiation exposure, and time resolutions of the samples. Encounters with cold clouds in our local neighborhood could be short-lived, since cold clouds within the Local Ribbon are estimated to be thin, filamentary sheets only 200 AU across. Some studies measuring cosmogenic isotopes have not detected cold cloud crossings 2-3 or 6-7 Mya, though these works use detection methods with 0.5 Myr temporal resolutions (Poluianov & Engelbrecht, 2025; Koll et al., 2025). We find that methods with these temporal resolutions, such as sampling of iron-manganese crusts, cannot detect short-lived crossings through clouds only a few hundreds of AU across; clouds must have parsec-scale sizes in order to be detectable using these records. Measurements of long-lived cosmogenic isotopes with high temporal resolutions, such as ^{10}Be measurements from ocean sediments, may be necessary to determine whether the Solar System crossed through small, dense interstellar cold clouds within the past few million years.

Open Research Section

Data is freely available at Nica et al. (2025).

Acknowledgments

This paper is based on work supported by NASA FINESST (grant number 80NSSC23K1638) and by NASA grant 18-DRIVE18.2 as part of the SHIELD DRIVE program, “Our Heliospheric Shield” (80NSSC22M0164, <https://shielddrivecenter.com/>).

References

Agostinelli, S., Allison, J., Amako, K., Apostolakis, J., Araujo, H., Arce, P., ...
 Zschieche, D. (2003, July). Geant4—a simulation toolkit. *Nuclear Instruments and Methods in Physics Research Section A: Accelerators, Spectrometers, Detectors and Associated Equipment*, 506(3), 250–303. Retrieved 2025-08-25, from <https://www.sciencedirect.com/science/article/pii/S0168900203013688>

doi: 10.1016/S0168-9002(03)01368-8

Allison, J., Amako, K., Apostolakis, J., Araujo, H., Arce Dubois, P., Asai, M., ... Yoshida, H. (2006, February). Geant4 developments and applications. *IEEE Transactions on Nuclear Science*, 53(1), 270–278. Retrieved 2025-08-25, from <https://ieeexplore.ieee.org/document/1610988> doi: 10.1109/TNS.2006.869826

Asefaw, H., Tauxe, L., Koppers, A. a. P., & Staudigel, H. (2021). Four-Dimensional Paleomagnetic Dataset: Plio-Pleistocene Paleodirection and Paleointensity Results From the Erebus Volcanic Province, Antarctica. *Journal of Geophysical Research: Solid Earth*, 126(2), e2020JB020834. Retrieved 2025-03-13, from <https://onlinelibrary.wiley.com/doi/abs/10.1029/2020JB020834> (_eprint: <https://onlinelibrary.wiley.com/doi/pdf/10.1029/2020JB020834>) doi: 10.1029/2020JB020834

Biggin, A. J., McCormack, A., & Roberts, A. (2010). Paleointensity Database Updated and Upgraded. *Eos, Transactions American Geophysical Union*, 91(2), 15–15. Retrieved 2025-10-22, from <https://onlinelibrary.wiley.com/doi/abs/10.1029/2010EO020003> (_eprint: <https://agupubs.onlinelibrary.wiley.com/doi/pdf/10.1029/2010EO020003>) doi: 10.1029/2010EO020003

Caballero-Lopez, R. A., & Moraal, H. (2004). Limitations of the force field equation to describe cosmic ray modulation. *Journal of Geophysical Research: Space Physics*, 109(A1). Retrieved 2024-07-25, from <https://onlinelibrary.wiley.com/doi/abs/10.1029/2003JA010098> (_eprint: <https://onlinelibrary.wiley.com/doi/pdf/10.1029/2003JA010098>) doi: 10.1029/2003JA010098

Comedi, E. S., Elias, A. G., & Zossi, B. S. (2020, December). Spatial features of geomagnetic cutoff rigidity secular variation using analytical approaches. *Journal of Atmospheric and Solar-Terrestrial Physics*, 211, 105475. Retrieved 2024-08-22, from <https://www.sciencedirect.com/science/article/pii/S1364682620302789> doi: 10.1016/j.jastp.2020.105475

Cummings, A. C., Stone, E. C., Heikkila, B. C., Lal, N., Webber, W. R., Jóhannesson, G., ... Porter, T. A. (2016, November). Galactic Cosmic Rays in the Local Interstellar Medium: Voyager 1 Observations and Model Results. *The Astrophysical Journal*, 831, 18. Retrieved 2024-05-14, from <https://ui.adsabs.harvard.edu/abs/2016ApJ...831...18C> (Publisher: IOP ADS Bibcode: 2016ApJ...831...18C) doi: 10.3847/0004-637X/831/1/18

Frank, M., Schwarz, B., Baumann, S., Kubik, P. W., Suter, M., & Mangini, A. (1997, June). A 200 kyr record of cosmogenic radionuclide production rate and geomagnetic field intensity from ^{10}Be in globally stacked deep-sea sediments1. *Earth and Planetary Science Letters*, 149(1), 121–129. Retrieved 2025-09-15, from <https://www.sciencedirect.com/science/article/pii/S0012821X97000708> doi: 10.1016/S0012-821X(97)00070-8

Golubenko, K., Rozanov, E., Kovaltsov, G., Leppänen, A.-P., Sukhodolov, T., & Usoskin, I. (2021, December). Application of CCM SOCOL-AERv2-BE to cosmogenic beryllium isotopes: description and validation for polar regions. *Geoscientific Model Development*, 14(12), 7605–7620. Retrieved 2025-06-06, from <https://gmd.copernicus.org/articles/14/7605/2021/> (Publisher: Copernicus GmbH) doi: 10.5194/gmd-14-7605-2021

Heikkilä, U., Beer, J., & Feichter, J. (2009, January). Meridional transport and deposition of atmospheric ^{10}Be . *Atmospheric Chemistry and Physics*, 9(2), 515–527. Retrieved 2025-01-27, from <https://acp.copernicus.org/articles/9/515/2009/acp-9-515-2009.html> (Publisher: Copernicus GmbH) doi: 10.5194/acp-9-515-2009

Koll, D., Lachner, J., Beutner, S., Fichter, S., Merchel, S., Rugel, G., ... Wallner, A. (2025, February). A cosmogenic ^{10}Be anomaly during the late

Miocene as independent time marker for marine archives. *Nature Communications*, 16(1), 866. Retrieved 2025-02-17, from <https://www.nature.com/articles/s41467-024-55662-4> (Publisher: Nature Publishing Group) doi: 10.1038/s41467-024-55662-4

Lal, D., & Peters, B. (1967). Cosmic Ray Produced Radioactivity on the Earth. In K. Sitte (Ed.), *Kosmische Strahlung II / Cosmic Rays II* (pp. 551–612). Berlin, Heidelberg: Springer. Retrieved 2025-10-22, from https://doi.org/10.1007/978-3-642-46079-1_7 doi: 10.1007/978-3-642-46079-1_7

Masarik, J., & Beer, J. (2009). An updated simulation of particle fluxes and cosmogenic nuclide production in the Earth's atmosphere. *Journal of Geophysical Research: Atmospheres*, 114(D11). Retrieved 2025-10-22, from <https://onlinelibrary.wiley.com/doi/abs/10.1029/2008JD010557> (eprint: <https://agupubs.onlinelibrary.wiley.com/doi/pdf/10.1029/2008JD010557>) doi: 10.1029/2008JD010557

Mewaldt, R. A., Cohen, C. M. S., Labrador, A. W., Leske, R. A., Mason, G. M., Desai, M. I., ... Haggerty, D. K. (2005, September). Proton, helium, and electron spectra during the large solar particle events of October–November 2003. *Journal of Geophysical Research (Space Physics)*, 110(A9), A09S18. doi: 10.1029/2005JA011038

Meyer, D. M., Lauroesch, J. T., Peek, J. E. G., & Heiles, C. (2012, June). The Remarkable High Pressure of the Local Leo Cold Cloud. *The Astrophysical Journal*, 752(2), 119. Retrieved 2025-03-12, from <https://dx.doi.org/10.1088/0004-637X/752/2/119> (Publisher: The American Astronomical Society) doi: 10.1088/0004-637X/752/2/119

Middleton, J., Pavia, F., Anderson, R., Schwartz, R., Fleisher, M., Lao, Y., ... Winckler, G. (2025, in review). Oceanographic and climatic controls of meteoric 10Be fluxes to seafloor sediments: A global synthesis. *Quaternary Science Reviews*.

Miyake, F., Nagaya, K., Masuda, K., & Nakamura, T. (2012, June). A signature of cosmic-ray increase in AD 774–775 from tree rings in Japan. *Nature*, 486(7402), 240–242. Retrieved 2025-09-22, from <https://www.nature.com/articles/nature11123> (Publisher: Nature Publishing Group) doi: 10.1038/nature11123

Morlino, G., & Gabici, S. (2015, July). Cosmic ray penetration in diffuse clouds. *Monthly Notices of the Royal Astronomical Society: Letters*, 451(1), L100–L104. Retrieved 2025-07-02, from <https://doi.org/10.1093/mnrasl/slv074> doi: 10.1093/mnrasl/slv074

Nica, A., Opher, M., Miller, J., & Middleton, J. (2025, November). *Data Supporting Nica et al. "Modeling Cosmogenic 10Be During the Heliosphere's Encounter with an Interstellar Cold Cloud"*. Zenodo. Retrieved 2025-11-12, from <https://zenodo.org/records/17594269> doi: 10.5281/zenodo.17594269

Opher, M., Giacalone, J., Loeb, A., Economo, E., Cummings, A., Middleton, J., ... Hatzaki, M. (2025, in review). Heliospheric Dynamics Driving Elevated Radiation Exposure of Earth 2–3 million years ago. *Scientific Reports*.

Opher, M., Loeb, A., Peek, J. E., Miller, J., Jennifer, M., & Nica, A. (2025, in review). Reply to "no indication for a strong increase in gcr intensity 2–3 myr ago from cosmogenic nuclides" by dominik koll et al. *Matter Arising, Nature Astronomy*.

Opher, M., Loeb, A., & Peek, J. E. G. (2024, June). A possible direct exposure of the Earth to the cold dense interstellar medium 2–3 Myr ago. *Nature Astronomy*, 1–8. Retrieved 2024-06-10, from <https://www.nature.com/articles/s41550-024-02279-8> (Publisher: Nature Publishing Group) doi: 10.1038/s41550-024-02279-8

Opher, M., Loeb, A., Zucker, C., Goodman, A., Konietzka, R., Worden, A. Z., ... Foley, M. M. (2024, September). The Passage of the Solar System through the

Edge of the Local Bubble. *The Astrophysical Journal*, 972(2), 201. Retrieved 2025-02-11, from <https://dx.doi.org/10.3847/1538-4357/ad596e> (Publisher: The American Astronomical Society) doi: 10.3847/1538-4357/ad596e

Pavlov, A. K., Blinov, A. V., Frolov, D. A., Konstantinov, A. N., Ostryakov, V. M., & Vasilyev, G. I. (2017, November). Spatial distribution of the atmospheric radionuclide production by galactic cosmic rays and its imprint in natural archives. *Journal of Atmospheric and Solar-Terrestrial Physics*, 164, 308–313. Retrieved 2025-02-24, from <https://www.sciencedirect.com/science/article/pii/S1364682617301645> doi: 10.1016/j.jastp.2017.09.016

Peek, J., Jencson, J., Rest, A., Clark, C., Clark, S., Fielding, D., ... Zenati, Y. (2025, February). A Path-Breaking Observation of the Cold Neutral Medium of the Milky Way Through Thermal Light Echoes. *Bulletin of the AAS*, 57(2). Retrieved 2025-09-11, from <https://baas.aas.org/pub/2025n2i174p08/release/1>

Poluianov, S., & Engelbrecht, N. E. (2025, February). Detectability of the passage of the heliosphere through an interstellar cloud with cosmogenic nuclides in lunar soil. *Astronomy & Astrophysics*, 694, A62. Retrieved 2025-02-07, from <https://www.aanda.org/10.1051/0004-6361/202452337> doi: 10.1051/0004-6361/202452337

Poluianov, S., Kovaltsov, G. A., Mishev, A. L., & Usoskin, I. G. (2016). Production of cosmogenic isotopes ^{7}Be , ^{10}Be , ^{14}C , ^{22}Na , and ^{36}Cl in the atmosphere: Altitudinal profiles of yield functions. *Journal of Geophysical Research: Atmospheres*, 121(13), 8125–8136. Retrieved 2025-01-07, from <https://onlinelibrary.wiley.com/doi/abs/10.1002/2016JD025034> (eprint: <https://onlinelibrary.wiley.com/doi/pdf/10.1002/2016JD025034>) doi: 10.1002/2016JD025034

Poluianov, S., Kovaltsov, G. A., & Usoskin, I. G. (2018, October). Solar energetic particles and galactic cosmic rays over millions of years as inferred from data on cosmogenic ^{26}Al in lunar samples. *Astronomy & Astrophysics*, 618, A96. Retrieved 2025-08-25, from <https://www.aanda.org/articles/aa/abs/2018/10/aa33561-18/aa33561-18.html> (Publisher: EDP Sciences) doi: 10.1051/0004-6361/201833561

Simon, Q., Thouveny, N., Bourlès, D. L., Bassinot, F., Savranskaia, T., & Valet, J.-P. (2018, May). Increased production of cosmogenic ^{10}Be recorded in oceanic sediment sequences: Information on the age, duration, and amplitude of the geomagnetic dipole moment minimum over the Matuyama–Brunhes transition. *Earth and Planetary Science Letters*, 489, 191–202. Retrieved 2025-09-15, from <https://www.sciencedirect.com/science/article/pii/S0012821X18300980> doi: 10.1016/j.epsl.2018.02.036

Stone, E. C., Cummings, A. C., Heikkila, B. C., & Lal, N. (2019, November). Cosmic ray measurements from Voyager 2 as it crossed into interstellar space. *Nature Astronomy*, 3(11), 1013–1018. Retrieved 2024-07-10, from <https://www.nature.com/articles/s41550-019-0928-3> (Publisher: Nature Publishing Group) doi: 10.1038/s41550-019-0928-3

Stone, E. C., Cummings, A. C., McDonald, F. B., Heikkila, B. C., Lal, N., & Webber, W. R. (2013, July). Voyager 1 Observes Low-Energy Galactic Cosmic Rays in a Region Depleted of Heliospheric Ions. *Science*, 341(6142), 150–153. Retrieved 2024-07-10, from <https://www.science.org/doi/10.1126/science.1236408> (Publisher: American Association for the Advancement of Science) doi: 10.1126/science.1236408

Vannier, H., Redfield, S., Wood, B. E., Müller, H.-R., Linsky, J. L., & Frisch, P. C. (2025, March). Mapping Our Path through the Local Interstellar Medium: High-resolution Ultraviolet Absorption Spectroscopy of Sight Lines along the Sun’s Historical Trajectory. *The Astrophysical Journal*, 981(2), 102. Retrieved 2025-09-11, from <https://dx.doi.org/10.3847/1538-4357/adb033> (Publisher: The

American Astronomical Society) doi: 10.3847/1538-4357/adb033

Vos, E. E., & Potgieter, M. S. (2015, December). New Modeling of Galactic Proton Modulation During the Minimum of Solar Cycle 23/24. *The Astrophysical Journal*, 815(2), 119. Retrieved 2024-07-01, from <https://dx.doi.org/10.1088/0004-637X/815/2/119> (Publisher: The American Astronomical Society) doi: 10.1088/0004-637X/815/2/119

Willenbring, J. K., & von Blanckenburg, F. (2010, May). Long-term stability of global erosion rates and weathering during late-Cenozoic cooling. *Nature*, 465(7295), 211–214. Retrieved 2025-09-15, from <https://www.nature.com/articles/nature09044> (Publisher: Nature Publishing Group) doi: 10.1038/nature09044

Zheng, M., Adolphi, F., Ferrachat, S., Mekhaldi, F., Lu, Z., Nilsson, A., & Lohmann, U. (2024). Modeling Atmospheric Transport of Cosmogenic Radionuclide ^{10}Be Using GEOS-Chem 14.1.1 and ECHAM6.3-HAM2.3: Implications for Solar and Geomagnetic Reconstructions. *Geophysical Research Letters*, 51(2), e2023GL106642. Retrieved 2025-01-22, from <https://onlinelibrary.wiley.com/doi/abs/10.1029/2023GL106642> (eprint: <https://onlinelibrary.wiley.com/doi/pdf/10.1029/2023GL106642>) doi: 10.1029/2023GL106642